

Research Paper

Stabilization of IGF2BP1 by USP10 promotes breast cancer metastasis via CPT1A in an m6A-dependent manner

Jiajun Shi^{1*}, Qianyi Zhang^{2*}, Xi Yin^{1*}, Jiahui Ye^{1*}, Shengqing Gao³, Chen Chen², Yaxuan Yang¹, Baojuan Wu¹, Yuping Fu⁴, Hongmei Zhang⁴, Zhangding Wang⁶, Bo Wang⁷, Yun Zhu⁶, Hongyan Wu⁵, Yongzhong Yao¹, Guifang Xu⁶✉, Qiang Wang⁸✉, Shouyu Wang^{2,7,9}✉, Weijie Zhang¹✉

1. Department of General Surgery, Nanjing Drum Tower Hospital, The Affiliated Hospital of Nanjing University Medical School, Nanjing 210000, Jiangsu Province, People's Republic of China.
2. Jiangsu Key Laboratory of Molecular Medicine, Medical School of Nanjing University, Nanjing 210000, Jiangsu Province, People's Republic of China.
3. Department of Neurosurgery, Jinling Hospital, Medical School of Nanjing University, Nanjing 210000, Jiangsu Province, People's Republic of China.
4. Nanjing Drum Tower Hospital Clinical College of Traditional Chinese and Western Medicine, Nanjing University of Chinese Medicine, Nanjing 210000, Jiangsu Province, People's Republic of China.
5. Department of Pathology, Nanjing Drum Tower Hospital, The Affiliated Hospital of Nanjing University Medical School, Nanjing 210000, Jiangsu Province, People's Republic of China.
6. Department of Gastroenterology, Nanjing Drum Tower Hospital, The Affiliated Hospital of Nanjing University Medical School, Nanjing 210000, Jiangsu Province, People's Republic of China.
7. Department of Hepatobiliary Surgery, Nanjing Drum Tower Hospital, The Affiliated Hospital of Nanjing University Medical School, Nanjing 210000, Jiangsu Province, People's Republic of China.
8. Department of Hepatobiliary Surgery, The First Affiliated Hospital of Anhui Medical University, Hefei 230022, Anhui Province, People's Republic of China.
9. Center for Public Health Research, Medical School of Nanjing University, Nanjing 210000, Jiangsu Province, People's Republic of China.

*These authors contributed equally to this work.

✉ Corresponding authors: Weijie Zhang, E-mail: zhangweijie1616@163.com; Shouyu Wang, E-mail: sywang@nju.edu.cn; Qiang Wang, E-mail: wangqiang@ahmu.edu.cn; Guifang Xu, E-mail: xuguifang@njgly.com.

© The author(s). This is an open access article distributed under the terms of the Creative Commons Attribution License (<https://creativecommons.org/licenses/by/4.0/>). See <http://ivyspring.com/terms> for full terms and conditions.

Received: 2022.07.04; Accepted: 2022.11.21; Published: 2023.01.01

Abstract

Metastasis leads to the vast majority of breast cancer mortality. Increasing evidence has shown that N6-methyladenosine (m6A) modification and its associated regulators play a pivotal role in breast cancer metastasis. Here, we showed that overexpression of the m6A reader IGF2BP1 was clinically correlated with metastasis in breast cancer patients. Moreover, IGF2BP1 promoted distant metastasis *in vitro* and *in vivo*. Mechanistically, we first identified USP10 as the IGF2BP1 deubiquitinase. USP10 can bind to, deubiquitinate, and stabilize IGF2BP1, resulting in its higher expression level in breast cancer. Furthermore, by MeRIP-seq and experimental verification, we found that IGF2BP1 directly recognized and bound to the m6A sites on CPT1A mRNA and enhanced its stability, which ultimately mediated IGF2BP1-induced breast cancer metastasis. In clinical samples, USP10 levels correlated with IGF2BP1 and CPT1A levels, and breast cancer patients with high levels of USP10, IGF2BP1, and CPT1A had the worst outcome. Therefore, these findings suggest that the USP10/IGF2BP1/CPT1A axis facilitates breast cancer metastasis, and this axis may be a promising prognostic biomarker and therapeutic target for breast cancer.

Key words: Breast cancer, metastasis, m6A, IGF2BP1, USP10, CPT1A

Introduction

Breast cancer (BC) has become the most commonly diagnosed cancer (11.7%) among all cancer cases, surpassing lung cancer (11.4%) for females in 2020 [1]. Moreover, female BC was the fifth leading cause of cancer death worldwide (6.9%) [1]. Metastasis occurs in more than 90% of all BC-related deaths [2-5]. The lungs, bones, brain, and liver are the most favourable BC metastatic sites [6-8]. However, the molecular mechanism of BC metastasis remains

unknown.

Epigenetic reprogramming is an important feature of BC cells with metastatic competence [9]. N6-Methyladenosine (m6A) modification is universally accepted to be the most pervasive and abundant RNA modification in eukaryotic RNAs [10] and has drawn much attention in recent years [11]. Increasing evidence has shown that m6A modification plays a pivotal role in cancer metastasis by regulating

RNA metabolism in tumour cells, cancer stem cells [12], tumour-associated macrophages [13], and others [10, 14]. The function of m6A modification has been widely reported in different cancers, including BC [15], gastrointestinal cancer (GC) [16, 17], ovarian cancer (OC) [18], and hepatocellular carcinoma (HCC) [12]. The methyltransferase complexes (“writers”) and demethylases (“erasers”) are responsible for the dynamic changes in m6A in specific transcripts. Methyltransferase complexes, including methyltransferase-like 3 (METTL3), METTL14, Wilms tumour 1-associated protein (WTAP), RBM15/15B, VIRMA (also called KIAA1429), and ZC3H13, catalyse the formation of m6A [19]. Demethylases, including fat mass and obesity-associated protein (FTO) and alkB homologue 5 (ALKBH5), selectively remove m6A from RNAs. Moreover, RNA-binding proteins (“readers”), including YTH domain-containing proteins (YTHDC1/2, YTHDF1/2/3), eukaryotic initiation factor 3 (eIF3), the IGF2 mRNA binding protein (IGF2BP1/2/3) families and the heterogeneous nuclear ribonucleoprotein (HNRNP) protein families, could affect the translation, splicing, exportation and stability of RNA by binding to and recognizing the m6A sites on RNA [20-22]. In particular, the m6A reader IGF2BP1 has been reported to function by promoting the stability of RNAs and upregulating numerous oncogenes dependent on m6A methylation [23-26]. Recently, the role of IGF2BP1 in the pathogenesis of BC metastasis has attracted much attention [27].

Ubiquitination, as a posttranslational modification, not only takes part in a large number of physiological events but also facilitates the origin and progression of cancer [28]. To date, the number of identified deubiquitinases (DUBs) is more than 100 [29]. By removing ubiquitin (Ub) from the substrate, DUBs can rescue the specific protein from being marked for degradation and maintain its protein level [28]. The deregulation of some DUBs is involved in the metastasis of BC [30-32]. Recently, the degradation of IGF2BPs has been reported to be related to the ubiquitin–proteasome system. However, the DUBs of IGF2BPs have not yet been discovered [33, 34].

In our study, we report the oncogenic role of IGF2BP1 in BC metastasis and identified USP10 as the deubiquitinase of IGF2BP1 for the first time. Moreover, we identified CPT1A, which has been reported to endow BC cells with the potential for metastasis [35-37], as the target gene of IGF2BP1. Based on our clinical prognostic data, BC patients with high expression levels of USP10, IGF2BP1, and CPT1A had the worst outcome. Therefore, our study uncovers an essential role of the USP10/IGF2BP1/CPT1A axis in the regulation of BC metastasis and

provides a promising prognostic biomarker and therapeutic target for BC patients with metastasis.

Materials and Methods

Patients and clinical samples

Examination of the signatures on the informed consent forms was exempted following the rules approved by the Ethics Committees of Nanjing Drum Tower Hospital and the Affiliated Hospital of Nanjing University Medical School. The cases in which patients were simultaneously suffering from other malignant diseases had previously been ruled out. In this study, 80 paraffin-embedded tissues obtained from the Department of Pathology of Nanjing Drum Hospital after BC resection from 2010 to 2019 were used. Two pathologists individually confirmed the results of haematoxylin and eosin (HE) staining and immunohistochemical (IHC) staining. The ages of the patients ranged from 27 to 74 years. The latest follow-up date was December 21, 2019.

Cell lines and cell culture

Human HEK293T, MDA-MB-468 and HCC1806 cells were obtained from the Shanghai Institute of Biochemistry and Cell Biology. The corresponding results with MDA-MB-231 cells and metastatic derivative cells LM2, BM6, and 1833 were described in a previous study [38]. HCC1806 cells were cultured in 1640 medium supplemented with 10% foetal bovine serum (FBS) and penicillin–streptomycin solution (Biochannel, Nanjing, China). Other cell lines were cultured in DMEM supplemented with 10% foetal bovine serum (FBS) and penicillin–streptomycin solution (Biochannel, Nanjing, China). All cells were cultured in an incubator with 5% CO₂ at 37 °C. Cells were stored at –80 °C using CELLSAVING (New Cell & Molecular Biotech, Suzhou, China).

Dot blot assay

This experiment followed the protocol in the bio-protocol database (<https://bio-protocol.org/e2095>). Briefly, mRNA isolated from the indicated cells was further denatured and then spotted onto a Hybond-N+ membrane and crosslinked by UV Crosslinker. After blocking the membrane, an anti-m6A antibody (1:1000; Abcam, USA) was incubated with the membrane overnight at 4 °C. Then, the membrane was further incubated with an HRP-conjugated anti-mouse antibody. Finally, images were recorded with a CCD camera (Tanon, Shanghai, China). Methylene blue (MB) was used to interact with mRNA and also used for normalization.

Transfection and lentiviral transduction

siRNAs targeting USP10 and CPT1A were

designed and synthesized by Genomeditech (Shanghai, China). Expressing plasmids, including USP1, USP2, USP3, USP4, USP5, USP7, USP8, USP10, USP11, USP12, USP13, USP14, USP15, USP16, USP17, USP18, USP20, USP21, USP22, USP26, USP28, USP32, USP33, USP36, USP37, USP38, USP39, USP43, USP44, USP45, USP46, USP47, USP48, USP49, USP50, USP51, USP52, USP54, COPS5, YOD1, BRCC3, EIF3F, VCIPI1, IGF2BP1 and CPT1A, with the indicated Flag- or HA-tags were constructed by Youbio (Hunan, China). Transfection of siRNA and plasmids was conducted using Lipofectamine 3000 (Invitrogen, USA). All siRNA sequences are listed in Supplementary Table 1.

Lentiviral plasmids carrying shIGF2BP1, shUSP10 and USP10 cDNA were designed and cloned into PGMLV-hU6-MCS-CMV-Luciferase-PGK-Puro, Cas9-Puro-U6 and PGMLV-CMV-MCS-3×Flag-EF1-ZsGreen1-T2A-Blasticidin, respectively, by Genomeditech (Shanghai, China). Forty-eight hours after lentiviral infection, cells were further selected with 2 µg/ml puromycin and 6 µg/ml blasticidin (Gibco). All target sequences are listed in Supplementary Table 1.

Mouse model of BC lung metastasis

Female BALB/c nude mice (4-5 weeks, 18-20 g) were purchased from GemPharmatech (Nanjing, China) and raised in a specific pathogen-free (SPF) experimental animal room. Treated cells (1×10^6 /100 µl PBS) were injected through the tail vein of the nude mice. Pulmonary metastasis was evaluated by bioluminescence imaging at 4 or 8 weeks. Then, the mice were sacrificed, and the lung tissues were imaged and fixed in 4% paraformaldehyde for further analyses.

RNA isolation and quantitative real-time PCR (qRT-PCR)

Total RNA was isolated from cultured cells using TRIzol reagent (Invitrogen), and reverse transcription was carried out by HiScript II Q RT SuperMix for qPCR (+gDNA wiper) (Vazyme) following the protocol provided by the manufacturer. The primers involved in the qRT-PCR experiments are listed in Supplementary Table 2. qRT-PCR was performed with 2 × ChamQ SYBR qPCR Green Master Mix (Vazyme Biotech Co., Ltd., Nanjing, China). The results were calculated by the $2^{-\Delta\Delta Ct}$ formula and normalized to the GAPDH levels.

RNA immunoprecipitation (RIP)

A MagnaRIP RNA-Binding Protein Immunoprecipitation Kit (Millipore, MA, USA) was used following the manufacturer's instructions. The cell lysates were incubated with beads coated with 5 µg of

control mouse IgG or anti-m6A antibody (Abcam, MA, USA) with gentle rotation at 4 °C overnight. Then, specifically captured products were obtained for the detection of CPT1A expression by qRT-PCR. The primers involved in the qRT-PCR experiments are listed in Supplementary Table 2.

Haematoxylin and eosin (HE) and immunohistochemical (IHC) staining

HE and IHC staining followed the standard protocols described in a previous study [39]. The results of IHC staining were evaluated considering both the staining intensity and proportion of tumour cells. The intensity was evaluated as follows: 0, negative; 1, weak; 2, moderate; and 3 strong. The proportion score was determined as follows: 0, less than 5%; 1, 5% to 25%; 2, 26% to 50%; 3, 51% to 75%; and 4, greater than 75%. The final IHC staining index was calculated by multiplying the two numbers (the final values ranged from 0 to 12).

Immunofluorescence (IF) assay

The indicated cells were seeded in a 24-well plate at a density of 2×10^4 cells per well. After 24 h, the cells were fixed with methanol for 15 min at room temperature and treated with 0.3% Triton X-100 for 15 min. After blocking for 30 min at room temperature, the indicated antibodies were added to the plate separately for incubation overnight at 4 °C. After being washed with PBS 3 times, the plate was further incubated with the secondary antibodies for 2 h at room temperature in the darkroom. DAPI was used to stain the nuclei. Finally, the cells were observed and imaged by fluorescence microscopy (LEICA DMi8, Germany).

Western blotting assay

Western blotting assays were performed according to standard protocols. Briefly, RIPA lysis buffer (P0013B, Beyotime) supplemented with protease inhibitor cocktail (P1005, Beyotime) and PMSF (ST507-10 ml, Beyotime) was used to lyse cells for 30 min at 4 °C. After centrifugation, the supernatants were collected. The protein concentration was also determined before western blotting. After resolving the proteins by SDS-polyacrylamide electrophoresis, the proteins were transferred to PVDF membranes. After the blotted membranes were blocked for 1 h, they were incubated with the indicated primary antibody overnight at 4 °C and then incubated with HRP-conjugated secondary antibodies for 1 h. Finally, the results were recorded by a CCD camera (Tanon, Shanghai, China) by ECL chemiluminescence (Millipore, Billerica, MA, USA). All antibodies are listed in Supplementary Table 3.

Transwell assay

The invasion and migration abilities of the cells were evaluated using Transwell chambers with 8 μm pore filters. After 48 h of transfection, cells ($3 \times 10^4/100 \mu\text{l}$) were seeded on the upper chambers coated with or without 70 μl of Matrigel (BD Biosciences) in serum-free DMEM. DMEM containing 10% FBS was added to the lower chambers. After incubation for 24 h at 37 °C, the cells in the chambers were collected and fixed with methanol or 4% paraformaldehyde. After removing the nonmigrating or noninvading cells with cotton swabs, the chambers were stained with crystal violet solution for 20 min. The results were recorded at $\times 200$ magnification under a microscope. All assays were repeated three times in duplicate.

RNA-seq and MeRIP-seq

RNA-seq and MeRIP-seq were performed by Gene Denovo (Guangzhou, China). Briefly, after extracting total RNA from LM2 cells with stable IGF2BP1 knockdown and the corresponding control cells, RNA was immunoprecipitated with an anti-m6A antibody and further used to construct RNA libraries, which were sequenced using Illumina NovaSeq™ 6000 by Gene Denovo Biotechnology Co. (Guang Zhou, China).

Statistical analysis

A paired t test or Wilcoxon signed-rank test was used to evaluate the mRNA levels of the major m6A-related enzymes in 112 breast cancer samples and the paired normal tissues from TCGA database. The differences in IGF2BP1 IHC staining indices in 11 primary breast tumours and the paired normal breast tissues were assessed by the Wilcoxon signed-rank test (grouped). Kaplan-Meier survival curves were analysed by the log-rank test. The correlations between the IHC staining indices of USP10 and IGF2BP1 were analysed by Spearman's test. Student's t test or conventional one-way ANOVA was used to identify statistically significant differences ($P < 0.05$) between the treated and control groups. GraphPad PRISM 8.0 was used to analyse all the data (GraphPad Software, La Jolla, CA, USA). All experiments were repeated three times. Data are shown as the mean \pm SD.

Results

Elevated IGF2BP1 expression resulted in poor prognosis of BC

To identify the roles of m6A regulators in BC, we first screened the expression of key m6A writers (METTL3, METTL14, and WTAP), erasers (ALKBH5

and FTO), and readers (YTHDC1, YTHDC2, YTHDF1, YTHDF3, IGF2BP1, IGF2BP2, and IGF2BP3) in BC samples and the paired normal breast tissues using The Cancer Genome Atlas (TCGA) data. The mRNA expression levels of YTHDC2, YTHDF1, YTHDF3, IGF2BP1, and IGF2BP3 were significantly increased in tumour tissues compared with paired normal breast tissues, while the METTL14, WTAP, FTO, and IGF2BP2 expression levels were significantly decreased in tumour tissues (Figure 1A). Correspondingly, the mRNA expression levels of METTL3, ALKBH5, and YTHDC1 showed no significant difference between the paired normal and BC tissues (Figure S1A). In addition, we examined all of these genes of interest in the BC tissues and paired controls in GEO datasets (GSE22820 and GSE86374) (Figure 1B). By taking the intersection of these results, we found that the mRNA expression levels of IGF2BP1, WTAP and FTO showed significant differences between the paired normal and BC tissues in all three datasets (Figure 1C). Among these three genes, only IGF2BP1 mRNA expression was associated with poor overall survival (OS) and disease-free survival (DFS) of BC patients based on TCGA datasets (Figure 1D and Figure S1C).

Furthermore, to explore the function of m6A modification in the metastasis of BC, we first detected the RNA m6A levels in MDA-MB-231, LM2 (MDA-MB-231 lung metastatic derivative), BM6 (MDA-MB-231 bone metastatic derivative), and 1833 (MDA-MB-231 brain metastatic derivative) cells. The RNA m6A levels were markedly increased in LM2, BM6, and 1833 cells compared with that in MDA-MB-231 cells as determined by dot blot assay (Figure 1E). Then, we examined the mRNA and protein expression levels of the key m6A writers (METTL3, METTL14, and WTAP), erasers (ALKBH5 and FTO), and readers (YTHDC1, YTHDC2, YTHDF1, YTHDF3, IGF2BP1, IGF2BP2, and IGF2BP3) in the four cell lines. Interestingly, the protein expression of IGF2BP1 was significantly higher in LM2, BM6, and 1833 cells than in MDA-MB-231 cells, but this phenomenon did not occur at the mRNA level (Figure 1F and Figure S1B).

We further confirmed this finding in our clinical samples and found elevated levels of the IGF2BP1 protein in BC tissues compared with paired normal breast tissues by immunohistochemical (IHC) staining ($n=11$; Figure 1G). To further evaluate the prognostic effect of IGF2BP1, we also assessed IGF2BP1 expression by IHC staining in 80 BC tissue samples. BC patients with higher IGF2BP1 expression had shorter OS and DFS (Figure 1H and Figure S1D). Moreover, primary BC tissues from patients with distant metastasis had higher expression of IGF2BP1

than those without distant metastases (n=7; Figure 1I). These data suggest that IGF2BP1 might play a crucial

role in the malignant process of BC, especially in its metastasis.

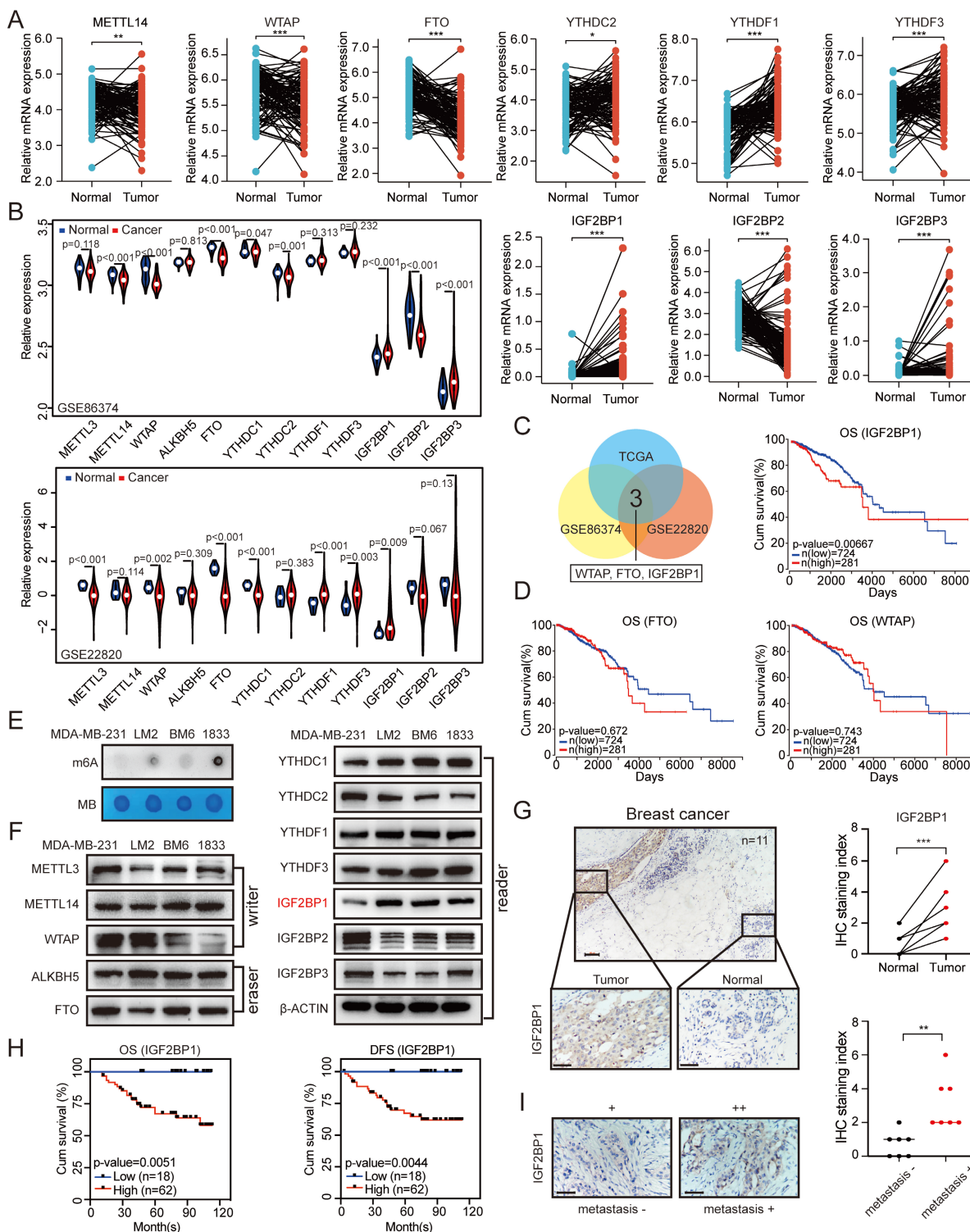


Figure 1. Elevated IGF2BP1 expression resulted in poor prognosis of BC. (A) The mRNA levels of m6A-related enzymes in 112 BC tissues and paired normal breast tissues from TCGA database (n=112, p<0.05, paired t test). (B) The mRNA levels of m6A-related enzymes in BC tissues and paired normal breast tissues from GEO datasets (GSE22820 and GSE86374). (C) Overlap of the differentially expressed genes of interest from TCGA dataset and the GEO datasets (GSE22820 and GSE86374). (D) Kaplan-Meier OS curves based on IGF2BP1, FTO and WTAP mRNA expression using the online bioinformatics tool based on TCGA. (E) RNAs isolated from MDA-MB-231, LM2, BM6, and 1833 cells were used in dot blot assays with an anti-m6A antibody. MB (methylene blue) served as a loading control. (F) Protein levels of m6A-related enzymes were measured in MDA-MB-231, LM2, BM6, and 1833 cells by western blotting. (G) Representative IHC staining images of the BC samples probed with an anti-IGF2BP1 antibody (scale bars=100 μm or 50 μm) (left panel). Calculated IHC staining indices of BC samples (right panel, n=11, p=0.0002, paired t test). (H) Kaplan-Meier DFS and OS analyses of IGF2BP1 expression in patients with BC (n=80, p<0.01, log-rank test). (I) Representative IHC staining images of the primary BC samples with or without metastasis probed with an anti-IGF2BP1 antibody (scale bars=50 μm) (left panel). Calculated IHC staining indices of BC samples (right panel, n=7, p=0.0031, unpaired t test). The data are represented as the means ± SEM. * p<0.05; ** p<0.01; *** p<0.001.

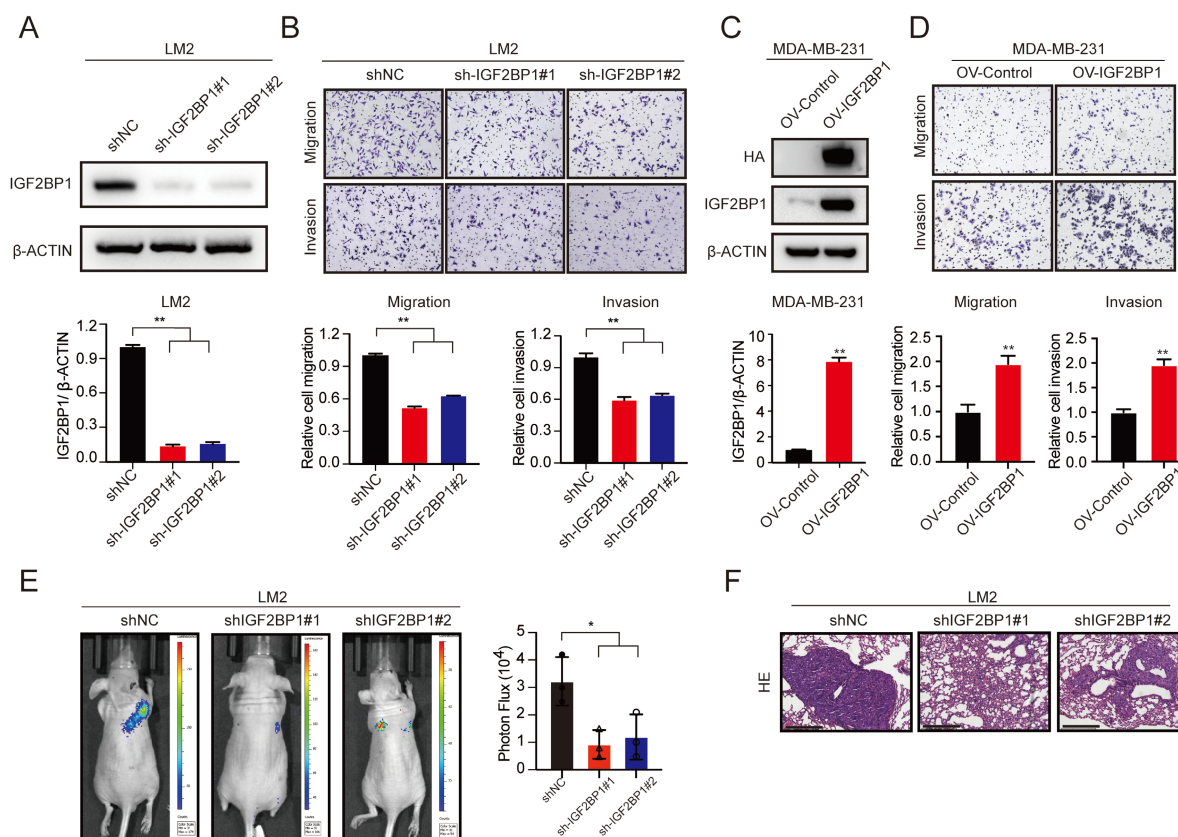


Figure 2. IGF2BP1 promoted breast cancer metastasis *in vitro* and *in vivo*. (A) The protein level of IGF2BP1 in LM2 cells with stable downregulation of IGF2BP1 measured by western blotting (upper panel). The grey values of the images were calculated using ImageJ (bottom panel). (B) Cell migration and invasion assays of LM2 cells deficient in IGF2BP1. Representative images and quantification of the cell migration and invasion assays are shown. (C) The protein levels of HA-tag and IGF2BP1 in MDA-MB-231 cells overexpressing IGF2BP1 measured by western blotting (upper panel). The grey values of the images were calculated using ImageJ (bottom panel). (D) Migration and invasion of MDA-MB-231 cells overexpressing IGF2BP1. Representative images and quantification of cell migration and invasion are shown. (E-F) IGF2BP1 downregulation led to markedly decreased BC lung metastasis in female nude mice (total n=9). Representative bioluminescence images and quantification of bioluminescence (E) of mice and HE staining (scale bars=275 μ m) (F) of pulmonary metastases 8 weeks after tail vein injection of IGF2BP1 downregulated or vector control LM2 cells. The data are represented as the means \pm SEM. * $p < 0.05$; ** $p < 0.01$; *** $p < 0.001$.

IGF2BP1 promoted BC metastasis *in vitro* and *in vivo*

To determine the role of IGF2BP1 in BC metastasis, we first established stable IGF2BP1 knockdown BC cells (LM2 and 1833) (Figure 2A and Figure S2A). The results showed that knockdown of IGF2BP1 suppressed the migration and invasion ability of LM2 and 1833 cells (Figure 2B and Figure S2B-C). In addition, we constructed IGF2BP1-overexpressing BC cells using the parental MDA-MB-231 cell line (Figure 2C). The results showed that ectopic expression of IGF2BP1 significantly promoted the migration and invasion ability of MDA-MB-231 cells (Figure 2D).

We further explored the prometastatic effect of IGF2BP1 *in vivo*. LM2-luciferase cells with IGF2BP1 knockdown and the corresponding control cells were injected into nude mice through the tail vein. Intriguingly, downregulation of IGF2BP1 significantly suppressed lung metastasis compared with that in the control group after 4 weeks, as indicated by bioluminescence imaging and haematoxylin and

eosin (HE) staining of pulmonary metastases (Figure 2E-F). These data suggest that IGF2BP1 may act as an oncogene that promotes BC metastasis.

USP10 bound to, deubiquitinated, and stabilized the IGF2BP1 protein

As shown in Figure 1F and Figure S1B, the IGF2BP1 protein level, but not the mRNA level, was higher in LM2 and 1833 cells than in MDA-MB-231 cells; therefore, we speculated that the IGF2BP1 protein may be more stable in metastatic BC cells. It has been reported that TRIM25, an E3 ubiquitin ligase, can regulate IGF2BP1 ubiquitination and degradation [33]. However, the deubiquitinase of IGF2BP1 is still unknown. To this end, we screened a panel of 43 DUBs (USP1, USP2, USP3, USP4, USP5, USP7, USP8, USP10, USP11, USP12, USP13, USP14, USP15, USP16, USP17, USP18, USP20, USP21, USP22, USP26, USP28, USP32, USP33, USP36, USP37, USP38, USP39, USP43, USP44, USP45, USP46, USP47, USP48, USP49, USP50, USP51, USP52, USP54, COPS5, YOD1, BRCC3, EIF3F, and VCP1P1) to investigate the potential interaction between each DUB and IGF2BP1 by coimmuno-

precipitation (co-IP) assays. We found that USP10 clearly bound to IGF2BP1 (Figure 3A). Furthermore, we discovered that exogenous USP10 and IGF2BP1 bound to each other in HEK293T cells using co-IP assays (Figure 3B-C), and endogenous USP10 and IGF2BP1 could interact in LM2 cells, MDA-MB-468

cells and HCC1806 cells (Figure 3D). In addition, as shown in Figure 3E, USP10 and IGF2BP1 were mainly colocalized in the cytoplasm. These data suggest that USP10 may function as the deubiquitinase of IGF2BP1.

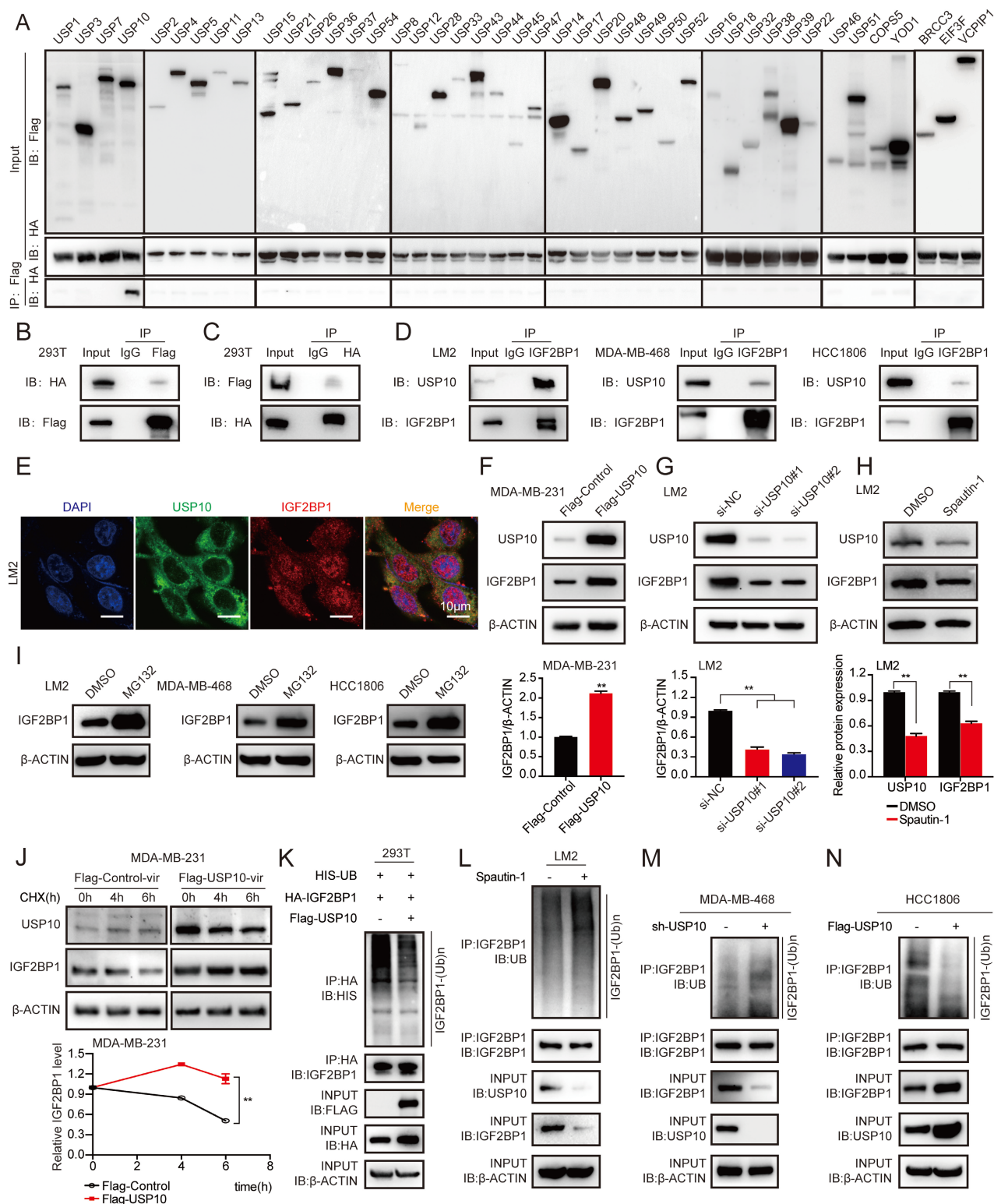


Figure 3. USP10 bound to and stabilized IGF2BP1 by deubiquitination. (A-C) USP10 specifically bound to IGF2BP1. HEK293T cells were transfected with FLAG-tagged DUBs and HA-tagged IGF2BP1 plasmids for 72 h, immunoprecipitated with FLAG or HA beads along with IgG control beads and then subjected to immunoblotting

(IB) with the indicated antibodies. (D) Endogenous USP10 bound to IGF2BP1 in LM2 cells, MDA-MB-468 cells and HCC1806 cells. Cell lysates from LM2 cells, MDA-MB-468 cells and HCC1806 cells were immunoprecipitated with an anti-IGF2BP1 antibody along with a normal IgG control, followed by IB with the indicated antibodies. (E) Immunofluorescence (IF) assays were used to detect the expression and location of USP10 and IGF2BP1 in LM2 cells (scale bars=10 μ m). (F-G) IGF2BP1 protein levels were detected by overexpressing or downregulating USP10 in MDA-MB-231 and LM2 cells. Cells were transfected with USP10 plasmids or siRNAs targeting USP10 for 48 h (upper panel). Densitometry quantification was carried out by ImageJ (bottom panel). (H) LM2 cells were treated with 10 μ M Spautin-1 for 6 h. The protein levels of USP10 and IGF2BP1 were measured by western blotting (upper panel). Grey value quantification was carried out by ImageJ (bottom panel). (I) LM2 cells, MDA-MB-468 cells and HCC1806 cells were treated with 10 μ M MG132 for 6 h, and the protein levels of IGF2BP1 were measured by western blotting. (J) USP10-overexpressing MDA-MB-231 cells and control cells were treated with 100 μ g/ml CHX for the indicated time periods. The protein levels of IGF2BP1 were measured by western blotting (upper panel). The decay curves are shown based on quantification of the grey values by ImageJ (bottom panel). (K) HEK293T cells were transfected with Flag-tagged USP10, Flag-tagged NC, HA-tagged IGF2BP1, and HIS-tagged UB plasmids for 72 h, followed by treatment with 10 μ M MG132 for 6 h. IGF2BP1 protein was pulled down by HA beads and then subjected to IB with the indicated Abs. (L) LM2 cells were treated with 10 μ M Spautin-1 for 6 h, followed by 10 μ M MG132 for 6 h. IGF2BP1 protein was pulled down and then subjected to IB with the indicated Abs. (M-N) USP10 was overexpressed or downregulated in MDA-MB-468 cells and HCC1806 cells followed by treatment with 10 μ M MG132 for 6 h. IGF2BP1 protein was pulled down and then subjected to IB with the indicated Abs. The data are represented as the means \pm SEM. * $p < 0.05$; ** $p < 0.01$; *** $p < 0.001$.

To determine whether USP10 could affect IGF2BP1 protein levels, USP10-overexpressing plasmids and their specific siRNAs were transfected into MDA-MB-231, LM2, and 1833 cells. Overexpression of USP10 elevated the expression of IGF2BP1 in MDA-MB-231 cells, while knockdown of USP10 reduced the protein level of IGF2BP1 in LM2 and 1833 cells (Figure 3F-G and Figure S3A-B). Additionally, IGF2BP1 protein expression was significantly decreased in LM2 cells treated with Spautin-1, a specific USP10 inhibitor [40] (Figure 3H). Meanwhile, we also examined the basal IGF2BP1 and USP10 expressions in MDA-MB-231, LM2, BM6, 1833, MDA-MB-468 and HCC1806 cells (figure S3C). Moreover, the IGF2BP1 protein level was increased in LM2 cells, MDA-MB-468 cells and HCC1806 cells treated with MG132, a proteasome inhibitor [41] (Figure 3I). Consistently, ectopic expression of USP10 prolonged the half-life of the IGF2BP1 protein in MDA-MB-231 cells treated with cycloheximide (CHX), a protein synthesis inhibitor [42] (Figure 3J). Furthermore, overexpression of USP10 decreased the level of ubiquitinated IGF2BP1 in LM2 cells compared with the corresponding control cells (Figure 3K). Inhibiting USP10 with Spautin-1 increased the level of ubiquitinated IGF2BP1 in LM2 cells compared with the corresponding control cells (Figure 3L). Moreover, we found that the level of ubiquitinated IGF2BP1 was enhanced or reduced in MDA-MB-468 cells and HCC1806 cells after USP10 knockdown or overexpression (Figure 3M-N and Figure S3D). Collectively, these results illustrated that the deubiquitinase USP10 interacted with IGF2BP1 and stabilized it at the protein level in BC cells.

The USP10/IGF2BP1 axis promoted BC metastasis *in vitro* and *in vivo*

The expression of USP10 was significantly upregulated in BC tissues compared with paired normal breast tissues based on TCGA data (Figure 4A). Moreover, higher expression of USP10 was associated with a poor prognosis of BC patients (Figure 4B). We performed IHC staining of 80 BC tissues and confirmed that higher USP10 expression was associated with shorter OS and DFS in BC

patients (Figure 4C-D and Figure S4A). As shown in Figure S4B, there was no significant relationship between the mRNA expression of USP10 and IGF2BP1. However, the protein level of USP10 were significantly correlated with that of IGF2BP1 in BC samples ($n=80$, $p < 0.001$, Figure 4E).

Subsequently, knocking down USP10 dramatically suppressed the migration and invasion of LM2 and 1833 cells (Figure 4F and Figure S4C-D). The USP10 inhibitor Spautin-1 also inhibited the migration of LM2 and 1833 cells (Figure 4G). Moreover, overexpressing IGF2BP1 markedly rescued the inhibition of migration caused by USP10 knockdown in LM2 and 1833 cells (Figure 4H and Figure S4E-F). Conversely, suppressing IGF2BP1 significantly blocked USP10 overexpression-induced migration in MDA-MB-231 cells (Figure 4I). Next, BC lung metastasis mouse models were constructed, and the number and size of lung metastatic lesions were analysed by bioluminescence imaging and HE staining of the pulmonary metastases at 8 weeks after injection. The results indicated that IGF2BP1 could block BC metastasis caused by USP10 overexpression *in vivo* (Figure 4J-K). These results suggest a pivotal role of the USP10/IGF2BP1 axis in BC metastasis.

IGF2BP1 recognized the m6A modification on CPT1A mRNA to maintain mRNA stability

To explore the molecular mechanism by which IGF2BP1 promoted BC metastasis, we performed methylated RNA immunoprecipitation sequencing (MeRIP-seq) and RNA sequencing (RNA-seq) in LM2 cells with stable IGF2BP1 knockdown and the corresponding control cells. The m6A peaks identified by MeRIP-seq were mainly distributed in the coding sequence (CDS), 3' untranslated region (3'UTR), start codon, and stop codon (Figure 5A). m6A occurs mostly in the RRACH (R=G or A, H=A, C, or U) consensus sequence [20, 43]. Our MeRIP-seq results revealed that the GGACT motif was highly enriched in the immunopurified RNA in both control LM2 cells and IGF2BP1 knockdown LM2 cells and the abundance of m6A was decreased in the mRNA of IGF2BP1 knockdown LM2 cells (Figure 5B). Furthermore, MeRIP-seq revealed that 6120

transcripts had fewer m6A peaks in IGF2BP1 knockdown cells than in control cells (fold change >1.5). Moreover, RNA-seq revealed that 300 transcripts were markedly decreased in IGF2BP1 knockdown cells compared with control cells (fold change >1.5) (Figure 5C and Figure S5A-B). Integrating the MeRIP-seq and RNA-seq results, 89 transcripts overlapped (Figure 5C). Furthermore, Kyoto Encyclopedia of Genes and Genomes (KEGG) enrichment analysis showed that these transcripts mainly functioned in the Hedgehog signaling pathway and PPAR signaling pathway (Figure 5D). Then, the expression of six candidate genes (CCND2, MEGF8, GLI3, CPT1A, ANGPTL4, PLIN4) in these two pathways was further verified in IGF2BP1-deficient LM2/1833 cells and IGF2BP1-overexpressing MDA-MB-231 cells by qRT-PCR (Figure 5F-G and Figure S5C). We found that the expression of CPT1A and GLI3 was consistently regulated by IGF2BP1 in these cells. Additionally, the m6A abundance in CPT1A and GLI3 mRNA was significantly decreased upon IGF2BP1 knockdown, as shown by the MeRIP-qPCR assay (Figure 5H and Figure S5D). Overexpression of IGF2BP1 also enriched the m6A abundance in CPT1A mRNA (Figure 5H). The Integrative Genomics Viewer (IGV) also indicated that the m6A levels on the exons of CPT1A mRNA were decreased in IGF2BP1 knockdown LM2 cells compared with control cells (Figure 5E). Moreover, the protein level of CPT1A was decreased in IGF2BP1 knockdown LM2/1833 cells but increased in IGF2BP1-overexpressing MDA-MB-231 cells compared with the corresponding control cells (Figure 5J-K). IGF2BP1 is recognized to stabilize target mRNA transcripts with m6A motifs [23]. We then treated IGF2BP1 knockdown LM2 cells and control cells with actinomycin D, an inhibitor of transcription [44], which showed that the mRNA level of CPT1A was less stable in IGF2BP1 knockdown LM2/1833 cells (Figure 5I). However, we found that knockdown of IGF2BP1 reduced m6A modification of GLI3, but did not affect GLI3 mRNA stability, indicating that IGF2BP1 may not completely depend on m6A modification to regulate GLI3 expression (Figure S5D-E). Together, our findings indicated that m6A modification maintains stable CPT1A expression in an IGF2BP1-dependent manner in metastatic BC cells.

IGF2BP1 promoted BC metastasis via the upregulation of CPT1A

To further characterize the function of CPT1A in BC metastasis, we first downregulated CPT1A with two different specific siRNAs and confirmed the knockdown efficiency by western blotting (Figure 6A and Figure S6A). In addition, MDA-MB-231 cells

stably overexpressing CPT1A were constructed (Figure 6B). We found that knockdown of CPT1A dramatically suppressed the migration and invasion abilities of LM2 and 1833 cells, while CPT1A overexpression promoted the migration and invasion abilities of MDA-MB-231 cells (Figure 6C-D and Figure S6B). Furthermore, ectopic expression of CPT1A rescued the decreased migration ability of IGF2BP1 knockdown LM2 and 1833 cells (Figure 6E&G and Figure S6C). Moreover, downregulating CPT1A by specific siRNAs blocked the enhanced migration abilities observed by overexpression of IGF2BP1 (Figure 6F&H). Thus, our data suggest that IGF2BP1 promoted BC metastasis by upregulating CPT1A expression.

Moreover, high expression of CPT1A mRNA also predicted poor OS of patients according to TCGA data (Figure 6I). Furthermore, IHC staining in 80 clinical BC samples confirmed that patients with higher CPT1A protein expression had shorter OS and DFS (Figure 6J-K and Figure S6D).

To further confirm the role of the USP10/IGF2BP1/CPT1A axis in BC metastasis, we analysed the IHC staining images of USP10, IGF2BP1, and CPT1A in our BC samples. As shown in Figure 7A, the USP10 levels distinctly correlated with the IGF2BP1 and CPT1A levels in BC tissues. Moreover, BC patients with high levels of USP10, IGF2BP1, and CPT1A had the worst outcomes compared with those with low levels of any or all of these indicators. (Figure 7B). These data suggest that the USP10/IGF2BP1/CPT1A axis may boost human BC progression and is correlated with BC patient survival.

Discussion

The decisive role of m6A modification in cancer progression has been widely reported in recent years [19, 45]. m6A modification is dynamically regulated by its writers, erasers, and readers, which are involved in the progression of cancer metastasis [13, 16, 46], including BC [15, 47-50]. Here, we found that the m6A reader IGF2BP1 was upregulated in BC tissues, especially BC metastatic lesions, and was associated with a poor prognosis of BC. Functionally, we first identified that the deubiquitinase USP10 could bind to and stabilize the IGF2BP1 protein, resulting in its high expression level in BC. Furthermore, IGF2BP1 directly bound to and recognized the m6A modification on CPT1A mRNA to maintain its stability, which had been reported to endow BC cells with the potential for metastasis [35, 37]. Thus, IGF2BP1 is capable of promoting BC distant metastasis (Figure 7C).

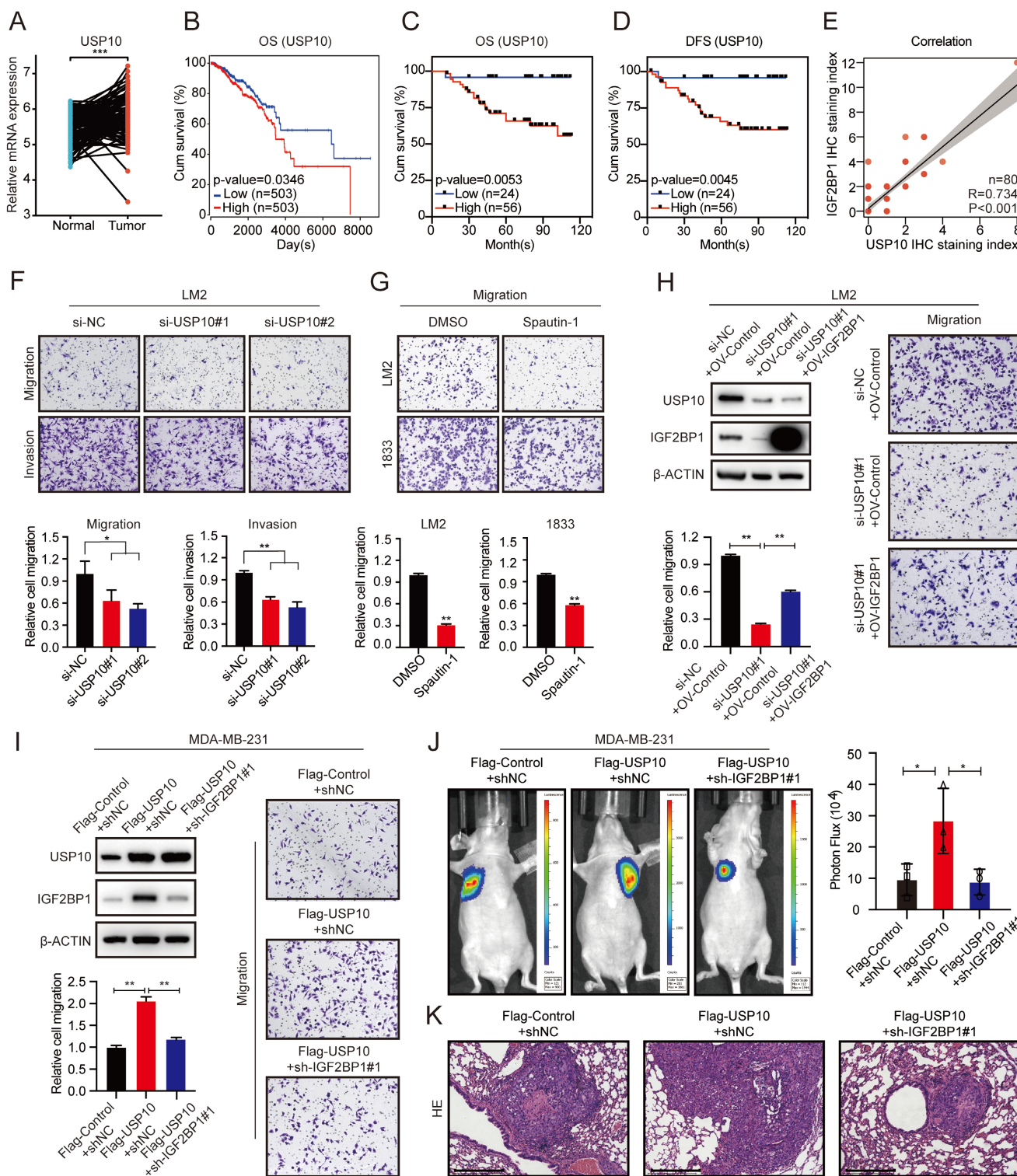


Figure 4. The USP10/IGF2BP1 axis promoted BC metastasis *in vitro* and *in vivo*. (A) USP10 mRNA expression in 112 BC tissues and paired normal breast tissues was analysed using TCGA data (n=112, p<0.001, paired t test). (B) Kaplan-Meier OS curves were analysed based on USP10 mRNA expression from TCGA data using the online bioinformatics tool. (C-D) Kaplan-Meier OS and DFS analyses of IGF2BP1 expression in patients with BC were performed (n=80, p<0.01, log-rank test). (E) The correlation between IGF2BP1 expression and USP10 expression in BC patients was analysed (n=80, p<0.001, Spearman test). (F-G) USP10 knockdown using targeting siRNAs or Spautin-1 effectively inhibited the migration and invasion abilities of LM2 cells or the migration ability of both LM2 and 1833 cells (upper panel). A graphical representation of the quantified data is shown (bottom panel). (H) IGF2BP1 overexpression rescued the reduced migration ability of LM2 cells caused by siRNAs targeting USP10. Representative images of the migration assays (right panel). Western blotting images and corresponding quantification of the migration assay (left panel). (I) Knockdown of IGF2BP1 inhibited the improved migration ability of MDA-MB-231 cells caused by USP10 overexpression. Representative images of migration assays (right panel). Western blotting and the corresponding quantification of migration ability results (left panel). (J) Downregulating IGF2BP1 blocked the enhanced metastatic ability of MDA-MB-231 cells induced by USP10 overexpression in female nude mice (total n=9). Representative bioluminescence images of mice 8 weeks after tail vein injection of treated MDA-MB-231 cells attached to the lung region and the corresponding quantification. (K) Corresponding HE staining images of pulmonary metastases (scale bars=275 µm). The data are represented as the means ± SEM. *p<0.05; **p<0.01; ***p<0.001.

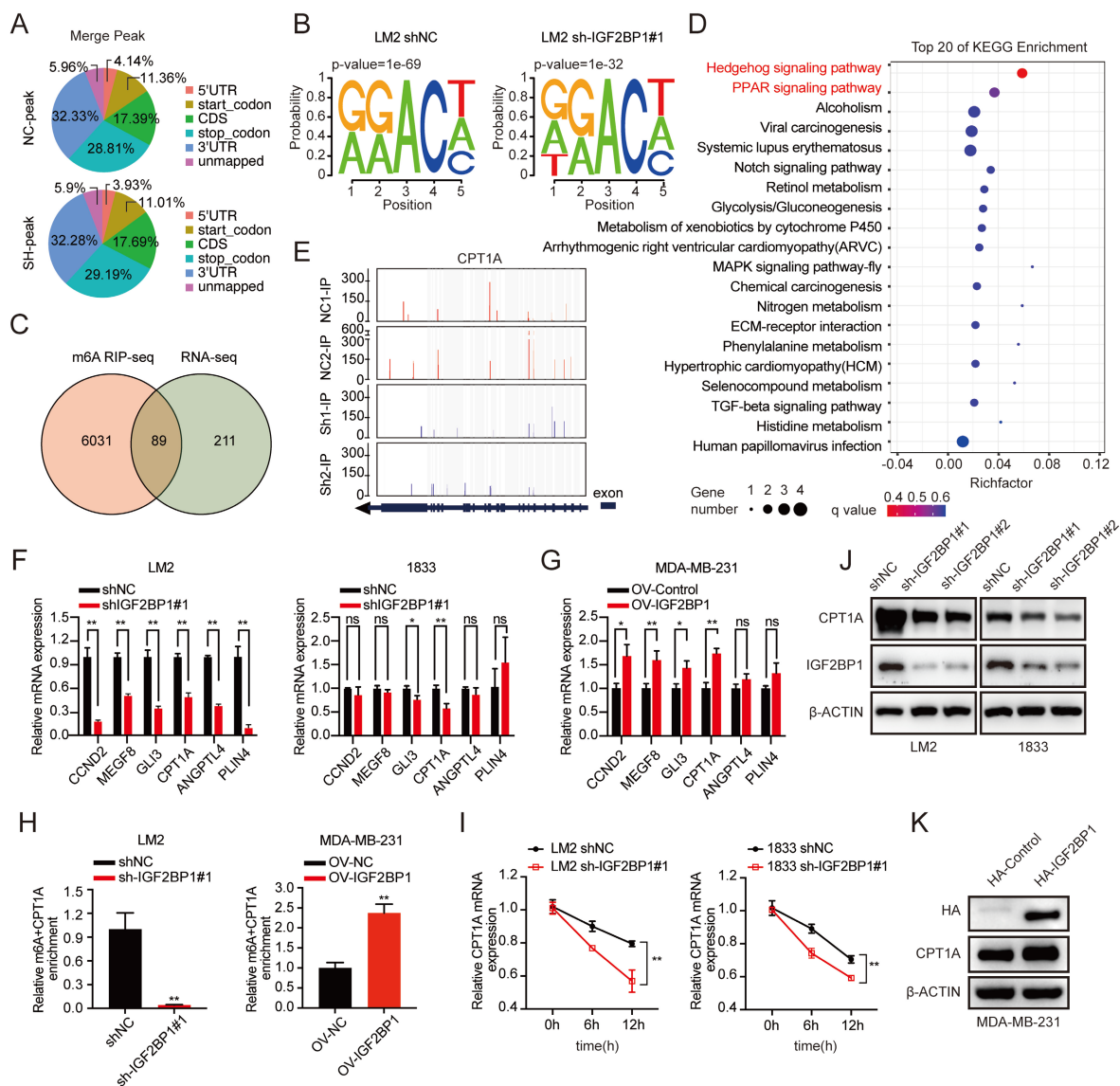


Figure 5. IGF2BP1 stabilized CPT1A via m6A modification. (A) The distribution of m6A peaks in each transcript segment of IGF2BP1 knockdown LM2 cells and vector control LM2 cells was analyzed. (B) Enrichment analyses for an averaged base frequency matrix based on the frequency distribution of a specific motif (RRACH) in IGF2BP1 knockdown and control LM2 cells performed by MeRIP-seq. (C) The overlapping differentially expressed genes determined by RNA-seq and MeRIP-seq performed using LM2 cells with stable knockdown of IGF2BP1 and compared with their corresponding controls. (D) The top 20 enriched KEGG pathways based on the overlapping genes in (C). (E) The m6A abundances detected by MeRIP-seq on CPT1A mRNA transcripts in IGF2BP1 knockdown LM2 cells and the corresponding control cells plotted by Integrative Genomics Viewer (IGV). (F-G) The mRNA expression levels of six candidate genes were examined in IGF2BP1 knockdown LM2/1833 cells (F) and IGF2BP1-overexpressing MDA-MB-231 cells (G) and compared with the corresponding control cells by qRT-PCR. (H) MeRIP-qPCR analysis was employed to demonstrate the decrease or increase in m6A modifications on CPT1A mRNA caused by IGF2BP1 downregulation and overexpression in LM2/MDA-MB-231 cells. (I) The mRNA expression of CPT1A was detected in IGF2BP1 knockdown LM2/1833 cells compared with the corresponding control LM2/1833 cells treated with actinomycin D (2 μg/mL) at the indicated time points by qRT-PCR. (J-K) The protein expression of CPT1A was examined in IGF2BP1 knockdown LM2 cells and 1833 cells and IGF2BP1-overexpressing MDA-MB-231 cells and compared with the corresponding control cells. The data are represented as the means ± SEM. * p<0.05; ** p<0.01; *** p<0.001.

IGF2BP1 is regarded as a classic RNA-binding protein involved in the regulation of gene expression [51, 52]. Recent evidence has confirmed that IGF2BP1 can function as an m6A reader to recognize m6A sites and enhance targeted mRNA stability [23]. Recently, IGF2BP1 was reported to promote BC lung metastasis by cooperating with METTL3 and FTO and stabilizing the keratin 7 (KRT7)-AS/KRT7 mRNA duplex by recognizing m6A at A877 on KRT7-AS [27]. Here, we first discovered that IGF2BP1 was upregulated in BC tissues, especially in BC patients with distant metastasis. Moreover, the IGF2BP1 protein level, but

not its mRNA level, was consistently elevated in the lung, bone, and brain BC metastatic derivative cell lines compared with the parental cell line, suggesting that IGF2BP1 plays an extensive role in the distant metastasis of BC.

The discrepancies of IGF2BP1 function in breast cancers need to be noted. It has been reported that IGF2BP1 functions as a tumor suppressor [53, 54]. However, recent studies from different research groups demonstrated the oncogenic roles of IGF2BP1 in breast cancer, maintaining the glycolysis and stemness of BCSCs through IGF2BP1/c-Myc axis [55,

56], promoting proliferation of breast cancer cells [57] and contributing the progression of breast cancer [58]. Based on GEO and TCGA datasets, Zhong et al. found that IGF2BP1 was an independent prognostic factor of breast cancer, and higher expression level of IGF2BP1 was associated with shorter overall survival of breast cancer patients [59], which was consistent with our

results. In our study, we found the oncogenic role of IGF2BP1 in TNBC cell lines, and we also showed that high expression of IGF2BP1 was clinically correlated with metastasis in breast cancer patients. Therefore, due to the complexity of the pathological types of breast cancer, more studies are warranted.

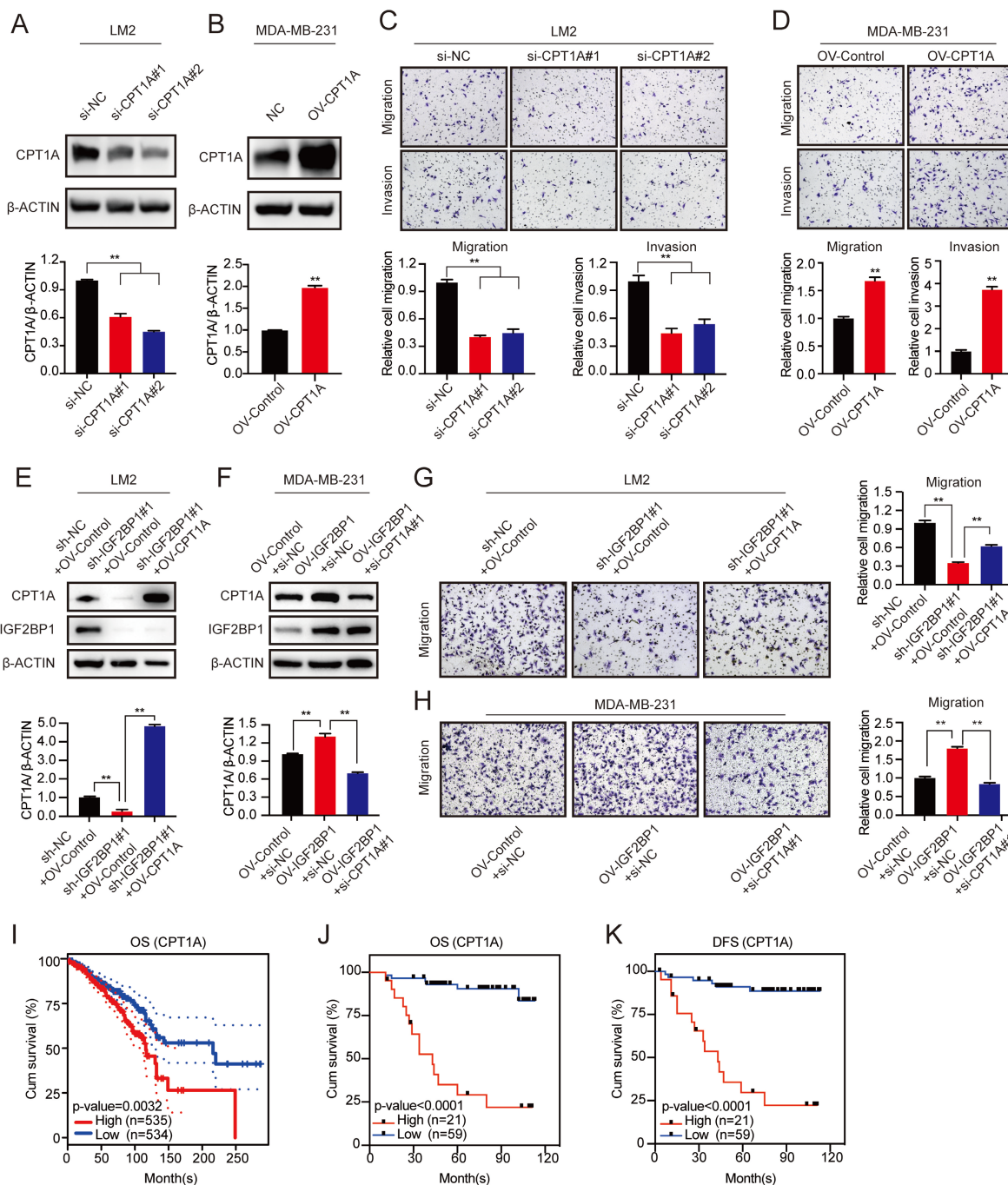


Figure 6. IGF2BP1 promoted BC metastasis by upregulating CPT1A. (A-B) CPT1A knockdown and overexpression efficiency verified by western blotting in LM2 cells (A) and MDA-MB-231 cells (B) (upper panel), and the corresponding quantification of the grey values (bottom panel). (C-D) Migration and invasion of LM2 cells with CPT1A knockdown (C) or MDA-MB-231 cells with CPT1A overexpression (D). Representative images (upper panel) and quantification (bottom panel) of cell migration and invasion are shown. (E&G) Upregulating CPT1A repaired the decreased migration ability of LM2 cells with stable knockdown of IGF2BP1 caused by targeting lentiviruses. Western blotting images and corresponding quantification analysis are shown (E). Representative images of migration assays and the corresponding quantification (G). (F&H) Knocking down CPT1A blocked the increased migration ability in IGF2BP1-overexpressing LM2 cells. The results of western blotting and corresponding quantification are shown (F). Representative migration assay results and the corresponding quantification are shown on the right (H). (I) Kaplan-Meier OS curves were analysed based on CPT1A mRNA expression using the online bioinformatics tool. (J-K) Kaplan-Meier OS and DFS analyses were carried out based on the CPT1A IHC staining indices in patients with BC (n=80, p<0.0001, log-rank test). The data are represented as the means ± SEM. * p<0.05; ** p<0.01; *** p<0.001.

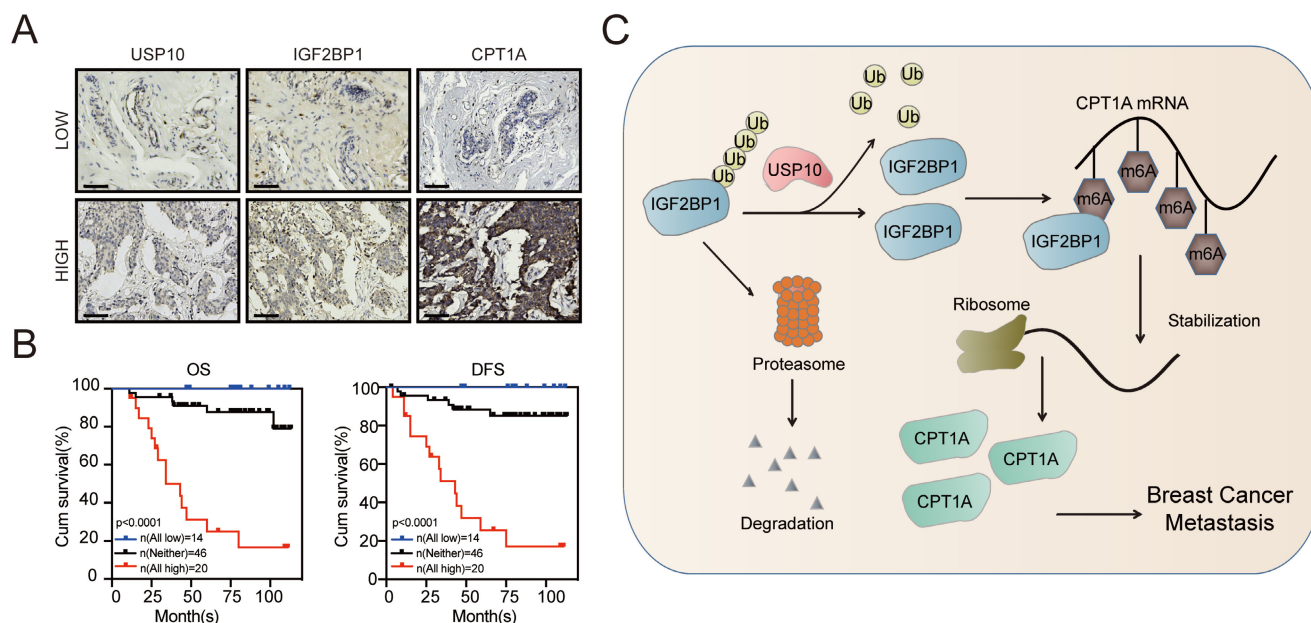


Figure 7. The clinical significance of the USP10/IGF2BP1/CPT1A axis in BC prognosis. (A) Representative IHC staining images of USP10, IGF2BP1, and CPT1A in the cancerous tissues of BC patients with high or low USP10 levels. **(B)** BC patients with high expression of USP10, IGF2BP1, and CPT1A had the lowest OS and DFS compared with the groups with low and no expression of these indicators. Kaplan-Meier OS and DFS analyses of 80 BC patients were performed (n=80, p<0.01, log-rank test). **(C)** The graphic illustrates that the USP10/IGF2BP1/CPT1A axis promoted BC metastasis.

The IGF2BP1 protein level has been reported to be widely upregulated in several aggressive cancers [27, 60-64]. However, the modulatory mechanisms underlying the abnormally elevated protein levels of IGF2BP1 in cancers are poorly understood. Previous studies have shown that posttranslational modification of some m6A regulators, such as ubiquitination [65], phosphorylation [66], sumoylation [67, 68], and lactylation [69, 70], could influence their biological function [33, 65, 71]. For example, F-box and WD repeat domain-containing 7 (FBW7), an E3-ubiquitin ligase, ubiquitinates YTHDF2 and suppresses tumour progression by antagonizing the tumour-promoting effect of YTHDF2 in ovarian cancer [72]. The ubiquitination of IGF2BP1/2/3 was first reported in their interaction with the E3-ubiquitin ligase tripartite motif-containing protein 25 (TRIM25) in non-small cell lung cancer (NSCLC) [33]. In addition, F-box/SPRY domain-containing protein 1 (FBXO45), an E3-ubiquitin ligase, was found to promote IGF2BP1 ubiquitination and attenuate hepatocellular carcinoma (HCC) progression [73]. However, the deubiquitinase of IGF2BP1 has not yet been reported. Our study first identified USP10 as the deubiquitinating enzyme of IGF2BP1, which maintained a high level of IGF2BP1 expression in BC. Moreover, we highlighted that USP10 was an independent prognostic marker that predicts the outcomes of BC patients.

Metabolic reprogramming is a hallmark of malignant tumours [74]. Fatty acid oxidation (FAO) is of great importance in tumour progression because it

increases the production of ATP and NADPH and enables cancer cells to survive under metabolic stress [75, 76]. In our previous study on oesophageal cancer (ESCA), the m6A reader HNRNP2B1 upregulated the expression of ATP citrate lyase (ACLY) and acetyl-CoA carboxylase (ACC1), two fatty acid synthetic enzymes, and promoted ESCA progression and metastasis [77]. In this study, by MeRIP and experimental verification, we first found that the FAO rate-limiting enzyme CPT1A [75, 78-80] was the downstream target of IGF2BP1. In colorectal cancer (CRC), CPT1A has been shown to strengthen resistance to anoikis and eliminate reactive oxygen species (ROS), thus promoting CRC cell metastatic capacity [79]. Here, we found that CPT1A mRNA could be stabilized by IGF2BP1 via recognition of its m6A modification, which led to its high level in BC and mediated IGF2BP1-induced distant metastasis in BC.

Conclusion

Our work revealed that the USP10/IGF2BP1/CPT1A axis promoted BC metastasis. In clinical samples, the USP10 levels were correlated with the IGF2BP1 and CPT1A levels in BC tissues, and BC patients with high levels of USP10, IGF2BP1, and CPT1A had the worst outcome. Therefore, the USP10/IGF2BP1/CPT1A axis might be a potential predictor and therapeutic target for BC.

Abbreviations

m6A: N6-Methyladenosine; IGF2BP1: IGF2

mRNA binding protein 1; USP: ubiquitin-specific protease; CPT1A: carnitine palmitoyl transferase 1 A; FAO: fatty acid oxidation; BC: breast cancer; GC: gastrointestinal cancer; OC: ovarian cancer; HCC: hepatocellular carcinoma; METTL3/14/16: methyltransferase-like 3/14/16; WTAP: Wilms tumor 1-associated protein; RBM15/15B: RNA-binding motif protein 15/15B; VIRMA: also called KIAA1429, vir-like m6A methyltransferase-associated; ZC3H13: zinc finger CCCH-type containing 13; FTO: fat mass and obesity-associated protein; ALKBH5: alkB homologue 5; eIF3: eukaryotic initiation factor 3; HNRNP: heterogeneous nuclear ribonucleoprotein; DUBs: deubiquitinating enzymes; Ub: ubiquitin; IHC: immunohistochemistry; HE: Hematoxylin and eosin; FBS: foetal bovine serum; MB: Methylene blue; COPS5: the fifth component of constitutive photomorphogenic-9 signalosome; YOD1: also known as OTU1, Ovarian tumor domain (OTU)-containing protein 1; BRCC3: BRCA1/BRCA2-containing complex subunit 3; VCIPI1: alosin-containing protein-interacting protein 1; SPF: specific pathogen free; RIP: RNA immunoprecipitation; IF: Immunofluorescence; OS: overall survival; DFS: disease free survival; TCGA: The Cancer Genome Atlas; MeRIP-seq: Methylated RNA immunoprecipitation sequencing; RNA-seq: RNA sequencing; KEGG: Kyoto Encyclopedia of Genes and Genomes; CCND2: cyclin D2; MEGF8: multiple epidermal growth factor-like domains 8; GLI3: glioma-associated oncogene homolog 3; CPT1A: carnitine palmitoyl-transferase 1A; ANGPTL4: angiotensin-like 4; PLIN4: perilipin 4; TNBC: triple negative breast cancer; Abs: antibodies; CHX: cycloheximide; IB: immunoblotting; IP: immunoprecipitation; DUBs: deubiquitylases; qRT-PCR: quantitative Real-time polymerase chain reaction; IGV: Integrative Genomics Viewer; F: Forward; R: Reverse.

Supplementary Material

Supplementary figures and tables.

<https://www.ijbs.com/v19p0449s1.pdf>

Acknowledgements

We are very grateful to TCGA datasets for providing valuable data resources.

Funding

This work was supported by the National Natural Science Foundation of China (81672380, 82273157, 81903085, 82073114, 82102984, and 82103266), the Project funded by China Postdoctoral Science Foundation (2020T130291, 2019M651808, and 2020M681562) and The Natural Science Foundation of Jiangsu Province (BK20200132). The work was also

supported by Nanjing special foundation for health science and technology development (distinguished young program, JQX21005).

Ethics statement

The use of human breast cancer tissues and the waiver of patient consent in this study were approved by the Clinical Research Review Board of Nanjing Drum Tower Hospital. The study was conducted according to the principles expressed in the Declaration of Helsinki. The animal studies were reviewed and approved by the Ethics Committee for Animal Studies at The First Affiliated Hospital of Nanjing Medical University.

Author contributions

JJ S, QY Z, X Y and JH Y contributed equally to this work. JJ S and QY Z performed the experiments; X Y and JH Y analyzed the data; YX Y, BJ W, YP F, and HM Z provided the clinical samples; SQ G, C C, and Y Z constructed lung metastasis models *in vivo*; HY W analyzed the pathological tissues; JJ S and Q W wrote the paper; WJ Z, SY W, Q W, GF X, YZ Y, ZD W, and B W commented on the study and revised the paper; WJ Z, SY W, Q W and GF X designed and supervised the research.

Data availability

Data are available upon reasonable request.

Competing Interests

The authors have declared that no competing interest exists.

References

- Sung H, Ferlay J, Siegel RL, Laversanne M, Soerjomataram I, Jemal A, et al. Global Cancer Statistics 2020: GLOBOCAN Estimates of Incidence and Mortality Worldwide for 36 Cancers in 185 Countries. *CA Cancer J Clin.* 2021; 71: 209-49.
- Eckhardt BL, Francis PA, Parker BS, Anderson RL. Strategies for the discovery and development of therapies for metastatic breast cancer. *Nat Rev Drug Discov.* 2012; 11: 479-97.
- Talmadge JE, Fidler IJ. AACR centennial series: the biology of cancer metastasis: historical perspective. *Cancer Res.* 2010; 70: 5649-69.
- Massagué J, Obenauf AC. Metastatic colonization by circulating tumour cells. *Nature.* 2016; 529: 298-306.
- Medeiros B, Allan AL. Molecular Mechanisms of Breast Cancer Metastasis to the Lung: Clinical and Experimental Perspectives. *Int J Mol Sci.* 2019; 20.
- Minn AJ, Gupta GP, Siegel PM, Bos PD, Shu W, Giri DD, et al. Genes that mediate breast cancer metastasis to lung. *Nature.* 2005; 436: 518-24.
- Bos PD, Zhang XHF, Nadal C, Shu W, Gomis RR, Nguyen DX, et al. Genes that mediate breast cancer metastasis to the brain. *Nature.* 2009; 459: 1005-9.
- Kang Y, Siegel PM, Shu W, Drobnjak M, Kakonen SM, Cordon-Cardo C, et al. A multigenic program mediating breast cancer metastasis to bone. *Cancer Cell.* 2003; 3: 537-49.
- Brooks MD, Burness ML, Wicha MS. Therapeutic Implications of Cellular Heterogeneity and Plasticity in Breast Cancer. *Cell Stem Cell.* 2015; 17: 260-71.
- Chen X-Y, Zhang J, Zhu J-S. The role of m6A RNA methylation in human cancer. *Mol Cancer.* 2019; 18: 103.
- Zhao BS, Roundtree IA, He C. Post-transcriptional gene regulation by mRNA modifications. *Nat Rev Mol Cell Biol.* 2017; 18: 31-42.
- Zhang C, Huang S, Zhuang H, Ruan S, Zhou Z, Huang K, et al. YTHDF2 promotes the liver cancer stem cell phenotype and cancer metastasis by regulating OCT4 expression via m6A RNA methylation. *Oncogene.* 2020; 39: 4507-18.

13. Yin H, Zhang X, Yang P, Zhang X, Peng Y, Li D, et al. RNA m6A methylation orchestrates cancer growth and metastasis via macrophage reprogramming. *Nat Commun.* 2021; 12: 1394.
14. Wang Q, Geng W, Guo H, Wang Z, Xu K, Chen C, et al. Emerging role of RNA methyltransferase METTL3 in gastrointestinal cancer. *J Hematol Oncol.* 2020; 13: 57.
15. Chang G, Shi L, Ye Y, Shi H, Zeng L, Tiwary S, et al. YTHDF3 Induces the Translation of mA-Enriched Gene Transcripts to Promote Breast Cancer Brain Metastasis. *Cancer Cell.* 2020; 38.
16. Yue B, Song C, Yang L, Cui R, Cheng X, Zhang Z, et al. METTL3-mediated N6-methyladenosine modification is critical for epithelial-mesenchymal transition and metastasis of gastric cancer. *Mol Cancer.* 2019; 18: 142.
17. Yang X, Zhang S, He C, Xue P, Zhang L, He Z, et al. METTL14 suppresses proliferation and metastasis of colorectal cancer by down-regulating oncogenic long non-coding RNA XIST. *Mol Cancer.* 2020; 19: 46.
18. Liu T, Wei Q, Jin J, Luo Q, Liu Y, Yang Y, et al. The m6A reader YTHDF1 promotes ovarian cancer progression via augmenting EIF3C translation. *Nucleic Acids Res.* 2020; 48: 3816-31.
19. Wang T, Kong S, Tao M, Ju S. The potential role of RNA N6-methyladenosine in Cancer progression. *Mol Cancer.* 2020; 19: 88.
20. Dominissini D, Moshitch-Moshkovitz S, Schwartz S, Salmon-Divon M, Ungar L, Osenberg S, et al. Topology of the human and mouse m6A RNA methylomes revealed by m6A-seq. *Nature.* 2012; 485: 201-6.
21. Roundtree IA, Evans ME, Pan T, He C. Dynamic RNA Modifications in Gene Expression Regulation. *Cell.* 2017; 169: 1187-200.
22. Wang Y, Li Y, Toth JI, Petroski MD, Zhang Z, Zhao JC. N6-methyladenosine modification destabilizes developmental regulators in embryonic stem cells. *Nat Cell Biol.* 2014; 16: 191-8.
23. Huang H, Weng H, Sun W, Qin X, Shi H, Wu H, et al. Recognition of RNA N-methyladenosine by IGF2BP proteins enhances mRNA stability and translation. *Nat Cell Biol.* 2018; 20: 285-95.
24. Liu L, Wu Y, Li Q, Liang J, He Q, Zhao L, et al. METTL3 Promotes Tumorigenesis and Metastasis through BMI1 mA Methylation in Oral Squamous Cell Carcinoma. *Mol Ther.* 2020; 28: 2177-90.
25. Ying Y, Ma X, Fang J, Chen S, Wang W, Li J, et al. EGR2-mediated regulation of mA reader IGF2BP proteins drive RCC tumorigenesis and metastasis via enhancing S1PR3 mRNA stabilization. *Cell Death Dis.* 2021; 12: 750.
26. Müller S, Glaß M, Singh AK, Haase J, Bley N, Fuchs T, et al. IGF2BP1 promotes SRF-dependent transcription in cancer in a m6A- and miRNA-dependent manner. *Nucleic Acids Res.* 2019; 47: 375-90.
27. Chen F, Chen Z, Guan T, Zhou Y, Ge L, Zhang H, et al. Methylenadenosine Regulates mRNA Stability and Translation Efficiency of KRT17 to Promote Breast Cancer Lung Metastasis. *Cancer Res.* 2021; 81: 2847-60.
28. Popovic D, Vucic D, Dikic I. Ubiquitination in disease pathogenesis and treatment. *Nat Med.* 2014; 20: 1242-53.
29. Grabbe C, Husnjak K, Dikic I. The spatial and temporal organization of ubiquitin networks. *Nat Rev Mol Cell Biol.* 2011; 12: 295-307.
30. Li W, Shen M, Jiang Y-Z, Zhang R, Zheng H, Wei Y, et al. Deubiquitinase USP20 promotes breast cancer metastasis by stabilizing SNAI2. *Genes Dev.* 2020; 34: 1310-5.
31. Qin J, Zhou Z, Chen W, Wang C, Zhang H, Ge G, et al. BAP1 promotes breast cancer cell proliferation and metastasis by deubiquitinating KLF5. *Nat Commun.* 2015; 6: 8471.
32. Liu S, González-Prieto R, Zhang M, Geurink PP, Kooij R, Iyengar PV, et al. Deubiquitinase Activity Profiling Identifies UCHL1 as a Candidate Oncoprotein That Promotes TGF β -Induced Breast Cancer Metastasis. *Clin Cancer Res.* 2020; 26: 1460-73.
33. Li B, Zhu L, Lu C, Wang C, Wang H, Jin H, et al. circNDUF2 inhibits non-small cell lung cancer progression via destabilizing IGF2BPs and activating anti-tumor immunity. *Nat Commun.* 2021; 12: 295.
34. Wang Y, Lu J-H, Wu Q-N, Jin Y, Wang D-S, Chen Y-X, et al. LncRNA LINRIS stabilizes IGF2BP2 and promotes the aerobic glycolysis in colorectal cancer. *Mol Cancer.* 2019; 18: 174.
35. Zeng F, Yao M, Wang Y, Zheng W, Liu S, Hou Z, et al. Fatty acid β -oxidation promotes breast cancer stemness and metastasis via the miRNA-328-3p-CPT1A pathway. *Cancer Gene Ther.* 2022; 29: 383-95.
36. Tan Z, Zou Y, Zhu M, Luo Z, Wu T, Zheng C, et al. Carnitine palmitoyl transferase 1A is a novel diagnostic and predictive biomarker for breast cancer. *BMC Cancer.* 2021; 21: 409.
37. Xiong Y, Liu Z, Li Z, Wang S, Shen N, Xin Y, et al. Long non-coding RNA nuclear paraspeckle assembly transcript 1 interacts with microRNA-107 to modulate breast cancer growth and metastasis by targeting carnitine palmitoyltransferase-1. *Int J Oncol.* 2019; 55: 1125-36.
38. Wu J, Jiang Z, Chen C, Hu Q, Fu Z, Chen J, et al. CircIRAK3 sponges miR-3607 to facilitate breast cancer metastasis. *Cancer Lett.* 2018; 430: 179-92.
39. Wang Q, Chen C, Ding Q, Zhao Y, Wang Z, Chen J, et al. METTL3-mediated mA modification of HDGF mRNA promotes gastric cancer progression and has prognostic significance. *Gut.* 2020; 69: 1193-205.
40. Liu J, Xia H, Kim M, Xu L, Li Y, Zhang L, et al. Beclin1 controls the levels of p53 by regulating the deubiquitination activity of USP10 and USP13. *Cell.* 2011; 147: 223-34.
41. Tawa NE, Odessey R, Goldberg AL. Inhibitors of the proteasome reduce the accelerated proteolysis in atrophying rat skeletal muscles. *J Clin Invest.* 1997; 100: 197-203.
42. Schneider-Poetsch T, Ju J, Eylar DE, Dang Y, Bhat S, Merrick WC, et al. Inhibition of eukaryotic translation elongation by cycloheximide and lactimidomycin. *Nat Chem Biol.* 2010; 6: 209-17.
43. Meyer KD, Salehore Y, Zumbo P, Elemento O, Mason CE, Jaffrey SR. Comprehensive analysis of mRNA methylation reveals enrichment in 3' UTRs and near stop codons. *Cell.* 2012; 149: 1635-46.
44. Cervantes-Gomez F, Nimmanapalli R, Gandhi V. Transcription inhibition of heat shock proteins: a strategy for combination of 17-allylamino-17-demethoxygeldanamycin and actinomycin d. *Cancer Res.* 2009; 69: 3947-54.
45. He L, Li H, Wu A, Peng Y, Shu G, Yin G. Functions of N6-methyladenosine and its role in cancer. *Mol Cancer.* 2019; 18: 176.
46. Peng W, Li J, Chen R, Gu Q, Yang P, Qian W, et al. Upregulated METTL3 promotes metastasis of colorectal cancer via miR-1246/SPRED2/MAPK signaling pathway. *J Exp Clin Cancer Res.* 2019; 38: 393.
47. Chen H, Yu Y, Yang M, Huang H, Ma S, Hu J, et al. YTHDF1 promotes breast cancer progression by facilitating FOXM1 translation in an m6A-dependent manner. *Cell Biosci.* 2022; 12: 19.
48. Xu Y, Ye S, Zhang N, Zheng S, Liu H, Zhou K, et al. The FTO/miR-181b-3p/ARL5B signaling pathway regulates cell migration and invasion in breast cancer. *Cancer Commun (Lond).* 2020; 40: 484-500.
49. Niu Y, Lin Z, Wan A, Chen H, Liang H, Sun L, et al. RNA N6-methyladenosine demethylase FTO promotes breast tumor progression through inhibiting BNIP3. *Mol Cancer.* 2019; 18: 46.
50. Shi W, Tang Y, Lu J, Zhuang Y, Wang J. MIR210HG promotes breast cancer progression by IGF2BP1 mediated m6A modification. *Cell Biosci.* 2022; 12: 38.
51. Hafner M, Landthaler M, Burger L, Khorshid M, Hausser J, Berninger P, et al. Transcriptome-wide identification of RNA-binding protein and microRNA target sites by PAR-CLIP. *Cell.* 2010; 141: 129-41.
52. Sun CY, Cao D, Du BB, Chen CW, Liu D. The role of Insulin-like growth factor 2 mRNA-binding proteins (IGF2BPs) as m(6)A readers in cancer. *Int J Biol Sci.* 2022; 18: 2744-58.
53. Nwokafor CU, Sellers RS, Singer RH. IMP1, an mRNA binding protein that reduces the metastatic potential of breast cancer in a mouse model. *Oncotarget.* 2016; 7: 72662-71.
54. Wang G, Huang Z, Liu X, Huang W, Chen S, Zhou Y, et al. IMP1 suppresses breast tumor growth and metastasis through the regulation of its target mRNAs. *Oncotarget.* 2016; 7: 15690-702.
55. Zhu P, He F, Hou Y, Tu G, Li Q, Jin T, et al. A novel hypoxic long noncoding RNA KB-1980E6.3 maintains breast cancer stem cell stemness via interacting with IGF2BP1 to facilitate c-Myc mRNA stability. *Oncogene.* 2021; 40: 1609-27.
56. Ma F, Liu X, Zhou S, Li W, Liu C, Chadwick M, et al. Long non-coding RNA FGF13-AS1 inhibits glycolysis and stemness properties of breast cancer cells through FGF13-AS1/IGF2BPs/Myc feedback loop. *Cancer Lett.* 2019; 450: 63-75.
57. Qiao YS, Zhou JH, Jin BH, Wu YQ, Zhao B. LINC00483 is regulated by IGF2BP1 and participates in the progression of breast cancer. *Eur Rev Med Pharmacol Sci.* 2021; 25: 1379-86.
58. Shi W, Tang Y, Lu J, Zhuang Y, Wang J. MIR210HG promotes breast cancer progression by IGF2BP1 mediated m6A modification. *Cell Biosci.* 2022; 12: 38.
59. Zhong S, Lin Z, Chen H, Mao L, Feng J, Zhou S. The m(6)A-related gene signature for predicting the prognosis of breast cancer. *PeerJ.* 2021; 9: e11561.
60. Bell JL, Wächter K, Mühleck B, Pazaitis N, Köhn M, Lederer M, et al. Insulin-like growth factor 2 mRNA-binding proteins (IGF2BPs): post-transcriptional drivers of cancer progression? *Cell Mol Life Sci.* 2013; 70: 2657-75.
61. Zhang L, Wan Y, Zhang Z, Jiang Y, Gu Z, Ma X, et al. IGF2BP1 overexpression stabilizes PEG10 mRNA in an m6A-dependent manner and promotes endometrial cancer progression. *Theranostics.* 2021; 11: 1100-14.
62. Liu Z, Wu G, Lin C, Guo H, Xu J, Zhao T. IGF2BP1 over-expression in skin squamous cell carcinoma cells is essential for cell growth. *Biochem Biophys Res Commun.* 2018; 501: 731-8.
63. Chen H-M, Lin C-C, Chen W-S, Jiang J-K, Yang S-H, Chang S-C, et al. Insulin-Like Growth Factor 2 mRNA-Binding Protein 1 (IGF2BP1) Is a Prognostic Biomarker and Associated with Chemotherapy Responsiveness in Colorectal Cancer. *Int J Mol Sci.* 2021; 22.
64. Stoskus M, Eidukaite A, Griskevicius L. Defining the significance of IGF2BP1 overexpression in t(12;21)(p13;q22)-positive leukemia REH cells. *Leuk Res.* 2016; 47: 16-21.
65. Sun H-L, Zhu AC, Gao Y, Terajima H, Fei Q, Liu S, et al. Stabilization of ERK-Phosphorylated METTL3 by USP5 Increases mA Methylation. *Mol Cell.* 2020; 80.
66. Schöller E, Weichmann F, Treiber T, Ringle S, Treiber N, Flatley A, et al. Interactions, localization, and phosphorylation of the mA generating METTL3-METTL14-WTAP complex. *RNA.* 2018; 24: 499-512.
67. Du Y, Hou G, Zhang H, Dou J, He J, Guo Y, et al. SUMOylation of the m6A-RNA methyltransferase METTL3 modulates its function. *Nucleic Acids Res.* 2018; 46: 5195-208.
68. Hou G, Zhao X, Li L, Yang Q, Liu X, Huang C, et al. SUMOylation of YTHDF2 promotes mRNA degradation and cancer progression by increasing its binding affinity with m6A-modified mRNAs. *Nucleic Acids Res.* 2021; 49: 2859-77.
69. Yu J, Chai P, Xie M, Ge S, Ruan J, Fan X, et al. Histone lactylation drives oncogenesis by facilitating mA reader protein YTHDF2 expression in ocular melanoma. *Genome Biol.* 2021; 22: 85.

70. Xiong J, He J, Zhu J, Pan J, Liao W, Ye H, et al. Lactylation-driven METTL3-mediated RNA m⁶A modification promotes immunosuppression of tumor-infiltrating myeloid cells. *Mol Cell*. 2022; 82.
71. Song W, Yang K, Luo J, Gao Z, Gao Y. Dysregulation of USP18/FTO/PYCR1 signaling network promotes bladder cancer development and progression. *Aging (Albany NY)*. 2021; 13: 3909-25.
72. Xu F, Li J, Ni M, Cheng J, Zhao H, Wang S, et al. FBW7 suppresses ovarian cancer development by targeting the N-methyladenosine binding protein YTHDF2. *Mol Cancer*. 2021; 20: 45.
73. Lin X-T, Yu H-Q, Fang L, Tan Y, Liu Z-Y, Wu D, et al. Elevated FBXO45 promotes liver tumorigenesis through enhancing IGF2BP1 ubiquitination and subsequent PLK1 upregulation. *Elife*. 2021; 10.
74. Hanahan D, Weinberg RA. Hallmarks of cancer: the next generation. *Cell*. 2011; 144: 646-74.
75. Qu Q, Zeng F, Liu X, Wang QJ, Deng F. Fatty acid oxidation and carnitine palmitoyltransferase I: emerging therapeutic targets in cancer. *Cell Death Dis*. 2016; 7: e2226.
76. An Y, Duan H. The role of m⁶A RNA methylation in cancer metabolism. *Mol Cancer*. 2022; 21: 14.
77. Guo H, Wang B, Xu K, Nie L, Fu Y, Wang Z, et al. m⁶A Reader HNRNPA2B1 Promotes Esophageal Cancer Progression via Up-Regulation of ACLY and ACC1. *Front Oncol*. 2020; 10: 553045.
78. Luo X, Cheng C, Tan Z, Li N, Tang M, Yang L, et al. Emerging roles of lipid metabolism in cancer metastasis. *Mol Cancer*. 2017; 16: 76-.
79. Wang Y-N, Zeng Z-L, Lu J, Wang Y, Liu Z-X, He M-M, et al. CPT1A-mediated fatty acid oxidation promotes colorectal cancer cell metastasis by inhibiting anoikis. *Oncogene*. 2018; 37: 6025-40.
80. Stoykova GE, Schlaepfer IR. Lipid Metabolism and Endocrine Resistance in Prostate Cancer, and New Opportunities for Therapy. *Int J Mol Sci*. 2019; 20.